Neuron, Vol. 28, 115–127, October, 2000, Copyright ©2000 by Cell Press

# Defective Neurogenesis in Citron Kinase Knockout Mice by Altered Cytokinesis and Massive Apoptosis

**Ferdinando Di Cunto,*# Sara Imarisio,* Emilio Hirsch,* Vania Broccoli,† Alessandro Bulfone,† Antonio Migheli,‡ Cristiana Atzori,‡ Emilia Turco,* Roberta Triolo,§ Gian Paolo Dotto,‖ Lorenzo Silengo,* and Fiorella Altruda***

*Department of Genetics, Biology and Biochemistry
University of Torino
Via Santena 5 bis, 10126, Torino
Italy

†Telethon Institute for Genetics and Medicine
HSR Biomedical Science Park
Via Olgettina 58, Milano
Italy

‡Department of Neuroscience
Laboratory of Neuropathology
University of Torino
Via Cherasco 15, Torino
Italy

§Dipartimento di Scienze Biomediche e Oncologia Umana
Via Santena 7, Torino
Italy

‖Cutaneous Biology Research Center
Massachusetts General Hospital and
Harvard Medical School
Charlestown, Massachusetts 02129

## Summary

**Citron-kinase (Citron-K) has been proposed by in vitro studies as a crucial effector of Rho in regulation of cytokinesis. To further investigate in vivo its biologic functions, we have inactivated *Citron-K* gene in mice by homologous recombination. *Citron-K*$^{-/-}$ mice grow at slower rates, are severely ataxic, and die before adulthood as a consequence of fatal seizures. Their brains display defective neurogenesis, with depletion of specific neuronal populations. These abnormalities arise during development of the central nervous system due to altered cytokinesis and massive apoptosis. Our results indicate that Citron-K is essential for cytokinesis in vivo but only in specific neuronal precursors. Moreover, they suggest a novel molecular mechanism for a subset of human malformative syndromes of the CNS.**

## Introduction

Development of the mammalian central nervous system (CNS) requires a tightly regulated sequence of cellular events involving the dynamic rearrangement of actin-rich cytoskeletal structures. These include cell proliferation, migration, and polarization, axon and dendrite outgrowth, axon pathfinding, and synaptogenesis. A great number of in vitro studies have shown that small GTPases of the Rho family are crucial regulators of the above-mentioned processes (Narumiya, 1996; Luo et al., 1997; Van Aelst and D'Souza-Schorey, 1997; Hall, 1998). However, their functions in the development and physiology of intact animals are still largely unknown.

The investigation of Rho GTPase actions during development of the mammalian CNS by loss-of-function mutants is complicated by two major obstacles: the possible functional redundancy between different family members (Valencia et al., 1991; Van Aelst and D'Souza-Schorey, 1997) and the potential pleiotropic effects of such mutations. Indeed, genetic targeting of Rho GTPases and their upstream regulators in various model organisms resulted in multiple developmental phenotypes, affecting gastrulation (Barrett et al., 1997; Sugihara et al., 1998), early morphogenesis (Magie et al., 1999; Wunnenberg-Stapleton et al., 1999), myoblast fusion (Luo et al., 1994), neuronal proliferation (Lee et al., 2000) and migration (Steven et al., 1998), dendrite outgrowth (Luo et al., 1996; Steven et al., 1998; Lee et al., 2000), axon outgrowth, and guidance (Luo et al., 1994; Steven et al., 1998).

Rho GTPases exert their complex functions through a network of effector proteins, which physically interact with the GTP-bound conformation and change their biologic activity upon binding (Narumiya et al., 1997; Hall, 1998). These molecules could work as integration points in Rho-dependent signal transduction pathways and play more restricted roles in the regulation of cytoskeletal dynamics (Van Aelst and D'Souza-Schorey, 1997). Henceforth, inactivation of specific effectors in mammals could be expected to be even more informative than targeting of any given GTPase.

Citron-N and Citron-K are two target molecules for activated Rho, produced by the same transcription unit (Di Cunto et al., 1998; Madaule et al., 1998). Citron-N was first identified for its ability to interact with GTP-bound Rho and Rac (Madaule et al., 1995). It is specifically expressed in the nervous system and is localized to postsynaptic densities, where it forms a stable complex with the membrane-associated guanylate kinase PSD-95 (Furuyashiki et al., 1999; Zhang et al., 1999). The functions of Citron-N are unknown, although it has been hypothesized that it may link the Rho signaling cascades to NMDA receptor complexes (Furuyashiki et al., 1999; Zhang et al., 1999).

Citron-K (also referred to as CRIK) is a longer variant of Citron-N, comprising an amino-terminal serine/threonine kinase domain (Di Cunto et al., 1998; Madaule et al., 1998). It shares a high degree of structural homology with the Rho-kinases (ROCKs) (Leung et al., 1996; Matsui et al., 1996; Nakagawa et al., 1996), and its activity is stimulated by activated Rho-A (Di Cunto et al., 1998). ROCKs and Citron-K have been implicated in control of cytokinesis downstream of Rho. Indeed, immunolocalization experiments have shown that they associate with the cleavage furrow and the midbody (Madaule et al., 1998; Kosako et al., 1999). Moreover, ROCKs appear

# To whom correspondence should be addressed (e-mail: dicunto@molinette.unito.it).

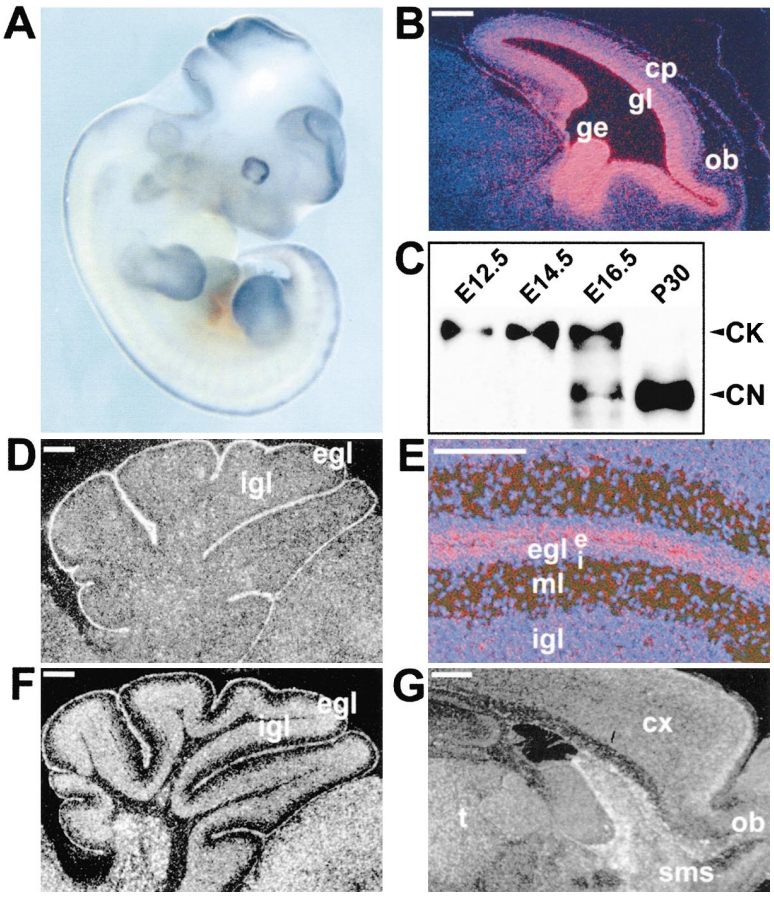


Figure 1. Expression of Citron-K and Citron-N during Development of Wild-Type Mouse CNS

(A) Lateral view of whole-mount ISH performed with probe K on an E11.5 mouse.

(B) Radioactive ISH performed with probe K on E14.5 sagittal section of telencephalon. *Citron-K* mRNA (pink) is restricted to the actively proliferating regions.

(C) Western blotting with anti-Citron antibodies, recognizing both Citron-K (CK) and Citron-N (CN). Samples were 30 μg of total proteins from embryonic telencephalon at the indicated stages and 5 μg from adult brain (P30). After higher exposure of the blot, CK was detected also in the P30 sample.

(D) Radioactive ISH performed with probe K on P12 cerebellum.

(E) High power field of (D) displays that *Citron-K* expression is restricted to the external part of the EGL.

(F) Radioactive ISH performed with probe C on P12 cerebellum. Besides labeling of the EGL, strong expression is detected in the IGL.

(G) Radioactive ISH performed with probe K on P12 telencephalon.

ge, ganglionic eminence; gl, germinal layer; cp, cortical plate; ob, olfactory bulb; egl, external germinal layer; e, external part; i, internal part; ml, molecular layer; igl, internal granular layer; cx, cerebral cortex; sms, subventricular migratory stream. Scale bars: 250 μm (B, D, F, and G); 50 μm (E).

to phosphorylate in a cytokinesis-dependent way the myosin binding subunit (MBS) of myosin light chain phosphatase (Kawano et al., 1999) and at least some classes of intermediate filaments (Kosako et al., 1997; Goto et al., 1998; Yasui et al., 1998). Nevertheless, functional in vitro studies, performed by overexpression of mutants and pharmacological inhibition in HeLa cells, suggested that only Citron-K is necessary for cytokinesis (Madaule et al., 1998).

In this report we have investigated the in vivo role played by Citron-K in mouse development. We have found that, during embryogenesis, it is abundantly expressed throughout the neuraxis, with a remarkable spatial restriction to proliferating areas. Moreover, when neuroblasts leave the cell cycle, Citron-K is downmodulated, while Citron-N becomes strongly expressed.

Mutant mice completely lacking Citron-K expression, but still producing normal levels of Citron-N, are affected by a complex neurological syndrome, characterized by severe ataxia and epilepsy, which bring them to death within the first 3 postnatal weeks. Their brains display dramatic neuronal depletion in the cerebral cortex and in the granular layers of cerebellum, hippocampus, and olfactory bulb. Abnormal cytokinesis and massive apoptosis were detected in the same brain regions during development of *Citron-K*$^{-/-}$ mice.

Our results demonstrate that Citron-K is indeed required for cytokinesis in vivo, but only in specific proliferating neuroblasts. Moreover, they strongly suggest that the induction of programmed cell death in *Citron-K*$^{-/-}$ neuroblasts is a direct consequence of the abnormal cytokinesis. Finally, our findings indicate a novel potential molecular basis for human brain malformative syndromes characterized by microcephaly and epilepsy.

## Results

### In the Developing CNS, Citron-K Is Expressed by Proliferating Precursors, Citron-N by Postmitotic Cells

Previous studies have revealed that, in the adult CNS, *Citron-N* is abundantly expressed by many neuronal populations, while *Citron-K* is expressed at much lower levels (Di Cunto et al., 1998; Furuyashiki et al., 1999). However, the expression pattern of the two different isoforms during development of the CNS was not reported. For this reason, we performed RNA in situ hybridization (ISH) on mouse embryos and postnatal brains using two different probes. The first (K) was derived from the kinase domain-coding sequence and specifically hybridizes with *Citron-K* transcript. The second (C) corresponds to a fragment of the coiled-coil region of Citron-K and reacts with both *Citron-N* and *Citron-K* mRNAs.

A clear signal was detected with both probes as early as embryonic day (E) 10.5. From this stage to E16.5, the highest expression levels were observed in the developing CNS (Figure 1A), with a noticeable spatial restriction to the proliferating areas of the entire neural tube (Figure 1B). Strong expression was also observed in limb buds and retina (Figure 1A). Lower expression was

detected in the other somatic organs already known to express Citron-K in the adult (Di Cunto et al., 1998; and data not shown).

Before E16.5, the hybridization pattern obtained with both probes was essentially identical (data not shown), thus suggesting that the predominant isoform produced in the mouse brain during neurogenesis is Citron-K. This was confirmed by analysis of Citron-N and Citron-K protein levels in brains at different developmental stages. Western blotting with antibodies raised against a common epitope revealed that before E16.5 the only isoform produced is Citron-K, at E16.5 they are both present, and in the adult brain Citron-N is by far the predominating isoform (Figure 1C).

In the first two postnatal weeks, robust expression of *Citron-K* was still detected by probe K in the external germinal layer (EGL) of the cerebellum (Figure 1D). During this period, cells of the cerebellar internal granular layer (IGL) are generated by proliferation and migration of precursor cells of the EGL (Goldowitz and Hamre, 1998). Strikingly, *Citron-K* was expressed only in the external part of the EGL, which contains the proliferating precursors (Figures 1E). It was not detectable in the IGL and in the internal part of the EGL, composed of postmitotic cells (Figures 1D and 1E). By contrast, probe C strongly labeled both the EGL and the IGL (Figure 1F), thus indicating high expression of Citron-N in differentiated cerebellar granules.

In the same period, relatively strong expression of *Citron-K* was also detected in the subventricular migratory stream (SMS; Figure 1G). This structure contains the precursors of olfactory bulb granules, which are still mitotically active while migrating toward their final location (Hinds, 1968).

Taken together, these data indicate that, within the CNS, Citron-K is specifically expressed by proliferating neuronal precursors, while postmitotic neuroblasts and differentiated neurons mainly express Citron-N.

### Generation of Citron-K-Deficient Mice

To directly address in vivo the specific role of Citron-K, we devised a gene targeting approach that would produce a null allele for this particular isoform and spare Citron-N expression.

mRNAs coding for both molecules are transcribed from the same gene (Di Cunto et al., 1998; Madaule et al., 1998), but so far it has not been defined if they are produced by alternative transcriptional initiation or alternative splicing. To clarify this point, we compared the available sequences of *Citron-K* and *Citron-N* 5′ untranslated regions (UTRs) and found no significant overlapping. Moreover, we assembled the complete genomic sequence of human *Citron-K* from three clones available in the public database (R. H. Waterston, GenBank accession numbers AC004813, AC004811, AC002563; Figure 2A) and compared it with mouse and rat *Citron-N* 5′ UTRs. This analysis revealed that all of the identified *Citron-N* 5′ noncoding exons map downstream of the kinase domain-coding region.

The above data argue against the alternative splicing mechanism and would be consistent with a second transcriptional initiation site for *Citron-N* downstream of the kinase domain-coding region.

For this reason, using homologous recombination in ES cells, we inserted a β-gal-Neo selection cassette within the second coding exon of mouse *Citron-K* (Figure 2B). Since the insertion point is far from the putative transcriptional initiation site of *Citron-N*, this mutation would be predicted to cause an early stop of *Citron-K* transcription and not to disturb *Citron-N* expression. Two independent ES cell clones were derived harboring the correct homologous recombination event (Figure 2C). Heterozygous (+/−) mice obtained from germline transmission of both ES clones were intercrossed to generate homozygous mutant (−/−) progeny.

Frequency at birth of the different genotypes obtained from +/− intercrossing was consistent with the expected Mendelian ratio (PCR analysis of a representative litter is shown in Figure 2D).

Western blotting with the above-mentioned antiserum confirmed complete loss of Citron-K expression in every analyzed tissue of −/− mice (Figure 2E). By contrast, compared to wild-type (+/+) littermate controls, Citron-N protein levels of *Citron-K*$^{-/-}$ brains were not decreased (Figure 2E), further confirming the existence of a second transcriptional initiation site.

### *Citron-K*$^{-/-}$ Mice Are Affected by a Complex Neurological Syndrome and Display Reduced Life Span for Lethal Epilepsy

Average weight and growth rate of *Citron-K*$^{-/-}$ mice did not differ significantly from +/− and +/+ littermates in the first postnatal week. However, failure to thrive became apparent around P10 in *Citron-K*$^{-/-}$ animals (at P12 the difference of body weight of −/− versus +/+ was 20%).

After P8 *Citron-K*$^{-/-}$ mice started to present an overt neurological phenotype, characterized by tremor and severe ataxia. At P12 *Citron-K*$^{-/-}$ mice were unable to stand for >2 s on a narrow (3 cm wide) platform, whereas littermate controls stayed balanced for >2 min. Their gait was wide and uncoordinated, and they were frequently falling on their backs while walking. Around the same age, *Citron-K*$^{-/-}$ mice became more irritable and started to present lethal seizures, characterized by myoclonic jerks followed by loss of posture, hyperextension of trunk and hindlimbs, and respiratory arrest. Occasionally, they were able to recover from crisis, but none of them survived beyond P21, with a peak of mortality observed at P14. No correlation was detected between body weight and mortality (data not shown).

To confirm the epileptic nature of crisis, we tested if *Citron-K*$^{-/-}$ mice had a lower threshold for seizures using the chemical convulsant pentylenetetrazol (PTZ) (Chae et al., 1997). P12 +/+ (n = 15) and +/− (n = 12) mice, injected intraperitoneally with PTZ, did not show seizure activity during the observation period. By contrast, 89% (n = 9) of *Citron-K*$^{-/-}$ mice displayed one or more seizures indistinguishable from those occurring spontaneously, with an average latency of 20 min from injection, and 78% died by the end of the observation period ($p < 0.001$, chi-square test).

### Brains of *Citron-K*$^{-/-}$ Mice Display Dramatic Depletion of Microneurons in the Olfactory Bulb, Hippocampus, and Cerebellum

Autopsy of *Citron-K*$^{-/-}$ mice did not reveal evidence of cerebral tumors, hemorrhage, or obvious disorders in

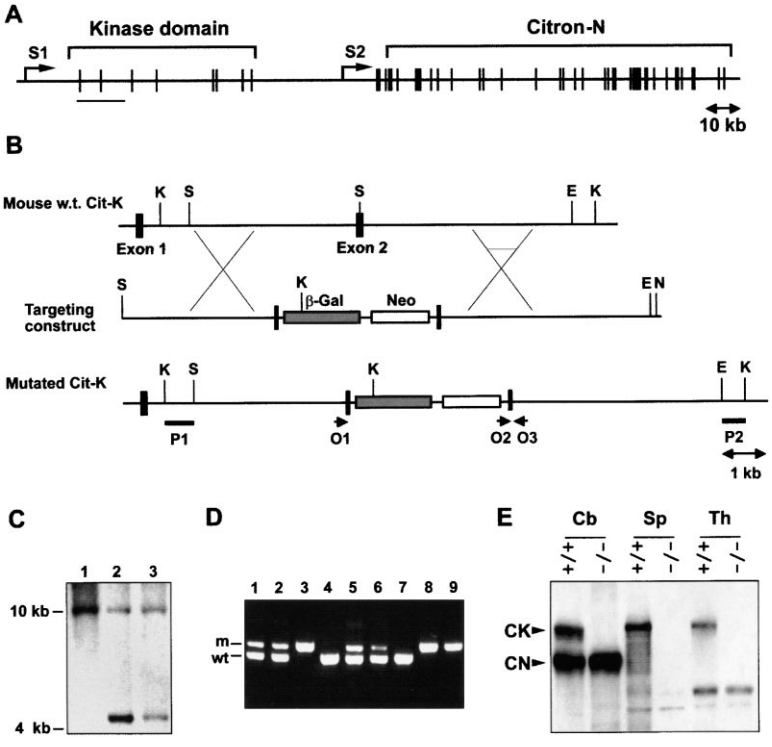


Figure 2. Gene-Targeting Strategy for the Specific Inactivation of *Citron-K*

(A) Schematic representation of the human *Citron-K* gene. S1 and S2 indicate the putative transcriptional initiation sites for *Citron-K* and *Citron-N* mRNAs, respectively. Underlining indicates the region homologous to the mouse sequence used for constructing the targeting vector.

(B) Structure of the wild-type mouse *Citron-K* locus, of the targeting construct, and of the mutated allele. Exons 1 and 2 are the first two coding exons of *Citron-K*. Lines P1 and P2 indicate the position of the 5′ and 3′ probes, respectively, used for Southern screening of ES cells and knockout mice. Arrows O1, O2, and O3 indicate the positions of primers used for routine genotyping of mice. K, KpnI; S, SmaI; E, EcoRI; N, NotI.

(C) Southern blotting with probe P1 of KpnI-digested genomic DNA from ES cell clones. Clones 2 and 3 presented the correct homologous recombination event.

(D) PCR performed with primers O1, O2, and O3 on a representative litter of *Citron-K*$^{+/-}$ mice, detecting wild-type (wt) and mutated (m) alleles.

(E) Western blotting with anti-Citron antibodies, performed on 30 μg of total proteins extracted from P5 cerebellum (Cb), spleen (Sp), and thymus (Th) of +/+ and −/− mice.

somatic tissues. However, macroscopic inspection of their brain showed a striking size reduction compared to control littermates (Figure 3A). At P14, the overall average weight of *Citron-K*$^{-/-}$ brains was reduced by 50% ($p < 0.01$). Dissection of principal brain areas revealed an average reduction of ~20% in diencephalon and midbrain, 50% in cerebral hemispheres, and 70% in cerebellum and olfactory bulbs. Histological examination showed that the structure of thalamus, hypothalamus, basal ganglia, and midbrain was preserved to a large extent, even though their cellularity was slightly reduced (Figure 3B and data not shown). Brain regions displaying the most abnormal structure in *Citron-K*$^{-/-}$ mice were the olfactory bulbs, the hippocampus, and the cerebellum (Figure 3B).

In the olfactory bulb of −/− mice, the number of glomeruli was approximately the same as in controls. However, instead of the normal monolayer organization, they formed a multilayer at the periphery of the bulb (Figure 3C). Based on morphologic criteria, the mitral cell layer was only slightly reduced. By contrast, periglomerular interneurons (PGI) and olfactory granular cells (OGR), as well as the external plexiform layer (EPL), were almost completely absent (Figure 3C). Accordingly, expression of the transcription factor *Dlx-2*, which specifically identifies PGI and OGR, (Bulfone et al., 1998) was barely detectable in the olfactory bulbs of *Citron-K*$^{-/-}$ mice (Figure 3D). A comparable cell depletion was observed in the SMS (Figure 3B).

In the hippocampus the Ammon's horn (AH) displayed normal lamination and cell density. By contrast, the dentate gyrus (DG) was almost completely missing (Figures 3B and 3E). Accordingly, calretinin immunoreactivity, which identifies DG granular cells, was strongly reduced in *Citron-K*$^{-/-}$ sections (Figure 3F).

In the cerebellum, all major lobules were recognizable, although they were strikingly smaller than in controls (Figure 3B). The number of Purkinje cells was not reduced, but their monolayer organization was disrupted and their dendritic harborization severely underdeveloped, as revealed by anti-calbindin immunostaining (Figure 3G). By contrast, the granular cell layer was dramatically reduced (Figures 3B and 3G). However, establishment of the cerebellar granule cell fate and differentiation was apparently conserved, as suggested by normal expression in the remaining granules of the transcription factor *NeuroD* (Miyata et al., 1999) (Figure 3H).

### Normal Regional Patterning and Specific Neuronal Deficits in *Citron-K*$^{-/-}$ Mice Cerebral Cortex

Average thickness of the cerebral cortex, measured on corresponding sagittal and coronal sections, was reduced by 40% in *Citron-K*$^{-/-}$ mice ($p < 0.01$). Based on morphological criteria, its laminar organization was only partially conserved. Layers 1, 5, and 6 could be easily recognized, but cells located above layer 5 were homogeneous for their shape and size (Figure 4A), thus making it difficult to distinguish layers 2, 3, and 4.

However, the expression pattern of the homeobox gene *Id-2* (Bulfone et al., 1995) showed that in *Citron-K*$^{-/-}$ brains the specification of cortical areas and layers was to a large extent preserved. In particular, a strong hybridization signal corresponding to layer 2, with a sharp rostro-caudal expression boundary, was present in both −/− and control animals (Figure 4B). Moreover, pyramidal neurons of layers 3 and 5 were easily identified by retrograde labeling with DiI crystals (Vercelli et al., 2000), indicating normal differentiation and connectivity (data not shown).

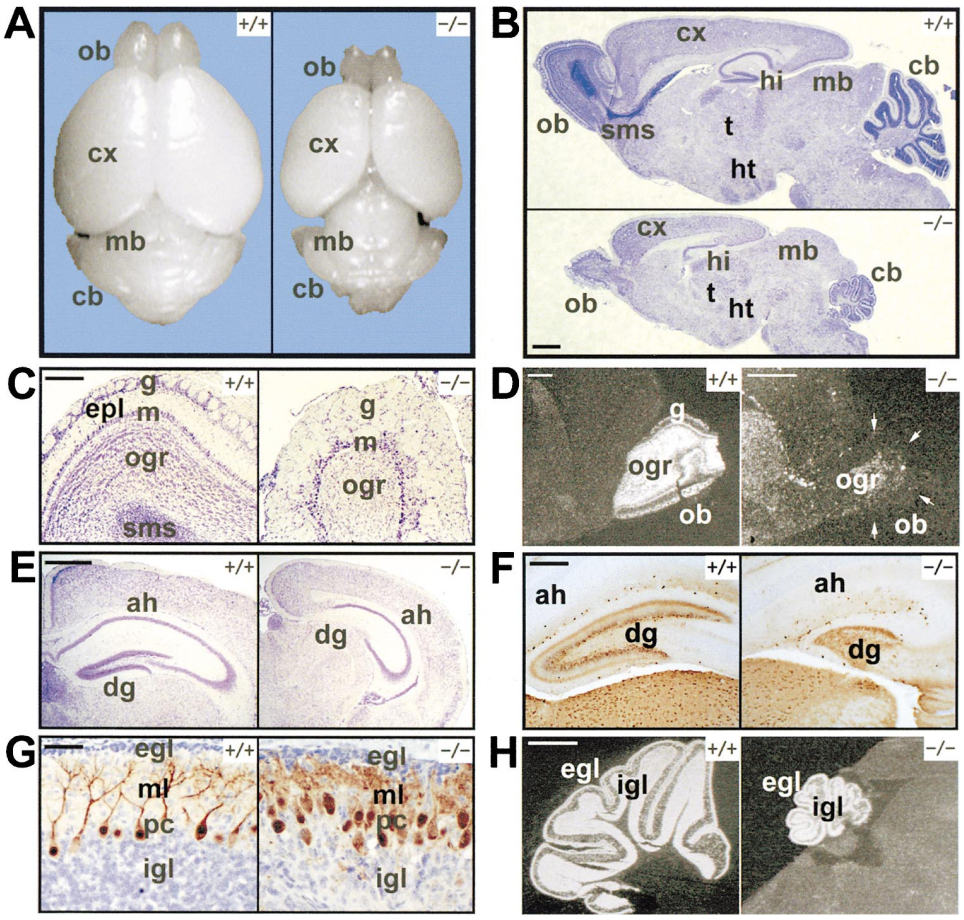


Figure 3. Specific Loss of Olfactory, Hippocampal, and Cerebellar Granules in Brains of *Citron-K*$^{-/-}$ Mice

(A) Dorsal view of P12 *Citron-K* +/+ and −/− brains.

(B) Sagittal sections of *Citron-K* +/+ and −/− brains stained with cresyl violet.

(C) Corresponding coronal sections of *Citron-K* +/+ and −/− olfactory bulb.

(D) Expression of the transcription factor *Dlx-2* detected by ISH on sagittal sections of olfactory bulbs from *Citron-K* +/+ and −/− mice. Arrows in the −/− panel indicate the margins of the olfactory bulb.

(E) Coronal sections of *Citron-K* +/+ and −/− hippocampus at the level of median eminence stained with cresyl violet.

(F) Anti-calretinin immunostaining of *Citron-K* +/+ and −/− hippocampus.

(G) Anti-calbindin immunostaining, counterstained with hematoxilin, of sagittal sections of *Citron-K* +/+ and −/− cerebellar cortex.

(H) Expression of the transcription factor *NeuroD* detected by ISH on sagittal sections of P12 cerebella from *Citron-K* +/+ and −/− mice.

mb, midbrain; cb, cerebellum; hi; hippocampus; sms, subventricular migratory stream; t, thalamus; ht, hypothalamus; g, olfactory glomeruli; epl, external plexiform layer; m, mitral cell layer; ogr, olfactory granules; ah, Ammon's horn; dg, dentate gyrus; pc, Purkinje cell layer. Scale bars: 1 mm (B, E, and H); 500 μm (D); 100 μm (C and F); 50 μm (G).

Cell density of layers 6 and 5 was slightly reduced (by 18% and 11%, respectively, $p < 0.05$). By contrast, layers above layer 5 were much more dramatically affected, with a 45% reduction ($p < 0.01$). The cortical GABA-containing interneurons were even more compromised. These cells are generated in the ganglionic eminence and reach their final location by tangential migration (Anderson et al., 1997). They can be identified during development as two sharp cortical stripes expressing the homeobox gene *Dlx-2* and after birth as calbindin-positive cells (Anderson et al., 1997). The *Dlx-2*-positive cell stripes could be easily identified at E14.5 in control animals but were almost absent in *Citron-K*$^{-/-}$ cortex (Figure 4C). Accordingly, in *Citron-K*$^{-/-}$ mice, the percentage of cortical calbindin-positive neurons was reduced by 70% at P12 (data not shown). Similar reduction was also observed for calretinin-positive interneurons (Figure 4D).

BrdU birth-dating experiments (Chae et al., 1997) did not reveal significant impairment of neuronal migration (our unpublished data).

Interestingly, in spite of high levels of Citron-K expression during the development of wild-type animals (Figure 1A), the structure and cellularity of retina and spinal cord in *Citron-K*$^{-/-}$ mice were comparable to littermate controls (data not shown).

### Normal DNA Synthesis and Massive Apoptosis in the Developing Brain of *Citron-K*$^{-/-}$ Mice

The expression of Citron-K in proliferating regions of the developing CNS and the reduction of cellularity observed in *Citron-K*$^{-/-}$ brains would suggest a prolifera-

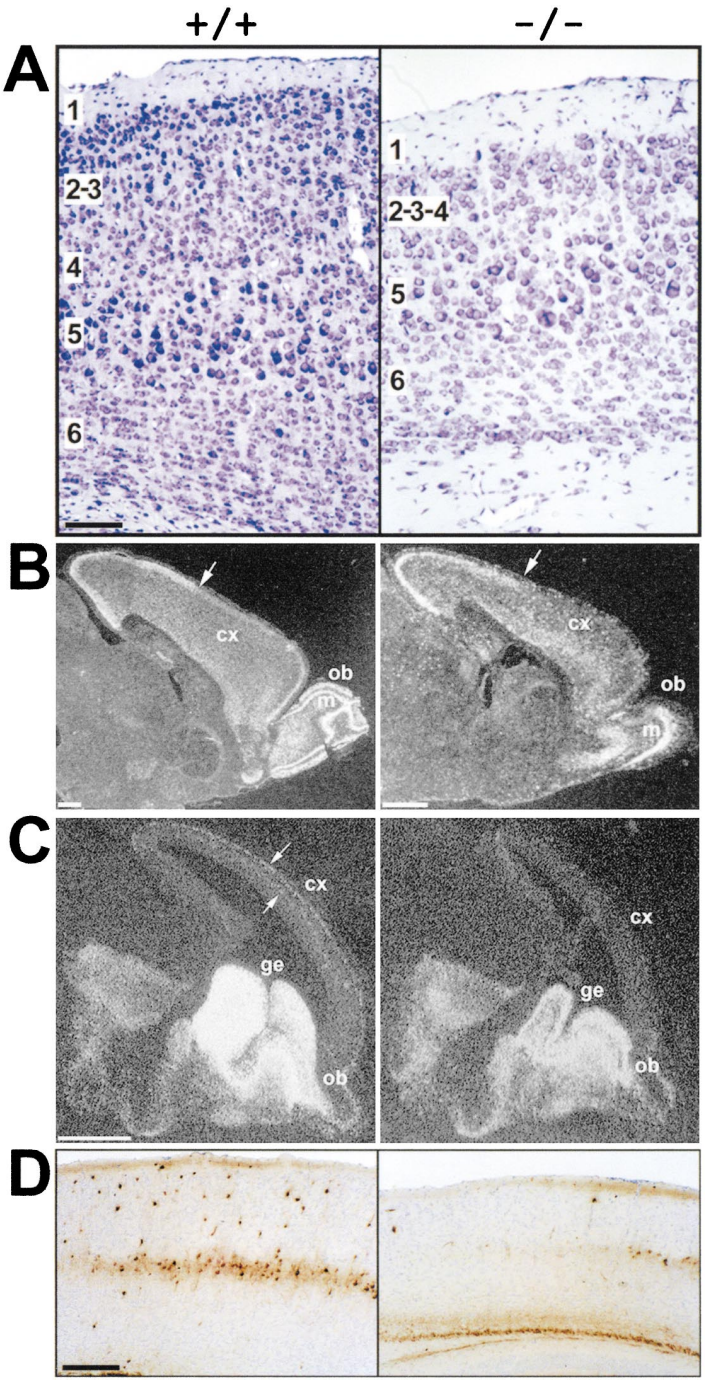


Figure 4. Structural Abnormalities of Cerebral Cortex in *Citron-K*$^{-/-}$ Mice

(A) Corresponding sagittal sections of *Citron-K* +/+ and −/− neocortex stained with cresyl violet. Numbers indicate the position of presumptive cortical layers.

(B) Expression of the transcription factor *Id-2* detected by ISH on sagittal sections of P12 brains from *Citron-K* +/+ and −/− mice. Arrows indicate the rostro-caudal expression boundary.

(C) Expression of the transcription factor *Dlx-2* detected by ISH on sagittal sections of E14.5 brains from *Citron-K* +/+ and −/− mice. Arrows in the +/+ panel indicate the positions of the positive cell stripes.

(D) Anti-calretinin immunostaining of coronal sections of *Citron-K* +/+ and −/− cerebral cortex. Scale bars: 1 mm (B and C); 250 μm (A); 100 μm (D).

tion deficit in neuroblast precursors. Alternatively, or in association, increased cell death could be involved.

To discriminate between these possibilities, serial sections from +/+ and −/− mice, at different stages of embryonic and postnatal development, were analyzed to reveal cells undergoing DNA synthesis or apoptotic cell death.

Before E11.5, no differences were observed between controls and *Citron-K*$^{-/-}$ animals. However, after this stage, a large number of pyknotic and fragmented nuclei, isolated or in clusters, were detected throughout the brain of −/− mice. These cells were strongly positive by TUNEL assay and activated Caspase-3 immunostaining (Srinivasan et al., 1998), indicating a massive apoptotic process (Figure 5A). At E14.5 apoptotic cells were particularly abundant in the ganglionic eminence and in the germinal and intermediate zones of the neocortex but were also detected in the cortical plate. At E16.5 apoptotic cells were identified in close proximity to the germinal regions of dentate gyrus and olfactory bulb granular layer (data not shown). Significant apoptosis was also detected in midbrain, pons, and medulla of E12.5–E16.5 animals. By contrast, the percentage and distribution of BrdU-positive cells was not significantly

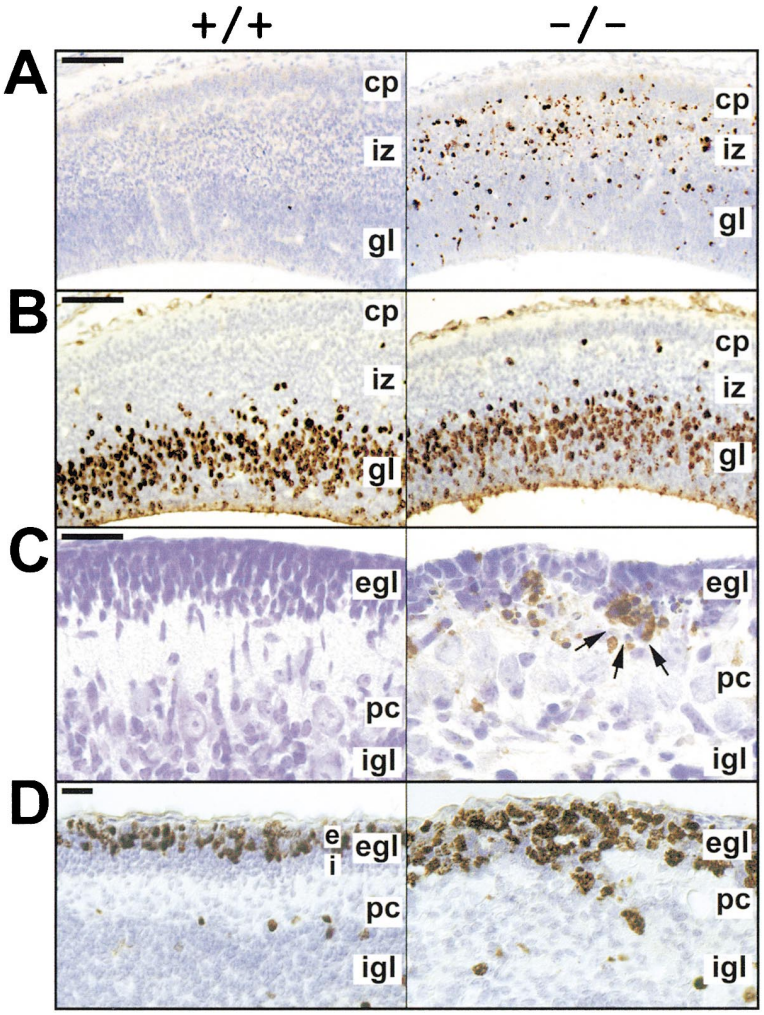


Figure 5. Normal DNA Synthesis and Massive Apoptosis during Development of CNS in *Citron-K*$^{-/-}$ Mice

(A) Sections of E14.5 cerebral cortex of *Citron-K* +/+ and −/− mice were analyzed by anti-activated Caspase-3 immunohistochemistry to detect apoptotic cells.

(B) Sections from the same embryos, previously labeled in utero by a 1 hr pulse of BrdU, were analyzed by BrdU immunohistochemistry to detect cells in S phase.

(C) TUNEL assay performed on sections of *Citron-K* +/+ and −/− cerebellar cortex at P8. Arrows in the −/− panel indicate an apoptotic cluster at the border between the EGL and Purkinje cell layer.

(D) Sections from the same cerebella, previously labeled for 1 hr with BrdU, analyzed by BrdU immunohistochemistry. iz, intermediate zone. Scale bars: 100 μm. (A and B); 50 μm (C and D).

different in −/− versus control samples at every analyzed stage (Figure 5B).

During the first 2 postnatal weeks, apoptotic cells were no longer detectable in the above-mentioned regions. In the same period, however, elevated levels of apoptosis were present in the EGL of cerebellum, especially at the border between the EGL and the Purkinje cell layer (Figure 5C). BrdU immunostaining revealed that in the EGL, the proliferating compartment was thicker than normal, but the postmitotic compartment was almost completely absent (Figure 5D).

These data suggest that Citron-K activity is required for survival of specific neuroblasts during a time window from the end of S phase until complete differentiation.

### Abnormal Cytokinesis during Neurogenesis of *Citron-K*$^{-/-}$ Mice

In consideration of the previous studies concerning Citron-K functions, cell losses observed in the development of *Citron-K*$^{-/-}$ brains could be related to abnormalities of cytokinesis. To test this hypothesis, we analyzed the DNA content of cells from *Citron-K*$^{-/-}$ and control tissues by flow cytometry.

Analysis of single-cell suspensions from thymus and spleen did not reveal significant differences in +/+ and −/− samples (data not shown). By contrast, a strong increase of tetraploid cells was detected in the developing cerebellum of *Citron-K*$^{-/-}$ mice (Figure 6A). At P12 diploid cells of +/+ and −/− cerebella were 94.4% and 47.3%, S phase cells 2.6% and 14.8%, tetraploid cells 3% and 37.9%, respectively (Figure 6A; $p < 0.0005$), thus indicating a dramatic block of knockout neuroblasts in the G2-M phase of the cell cycle. Similar results were obtained in cerebellum throughout the first 2 postnatal weeks. Careful analysis of the G2-M peak of *Citron-K*$^{-/-}$ samples revealed that it contained, besides tetraploid cells, a significant under-tetraploid population (Figure 6A).

A lower but consistent ($p < 0.005$) increase in the percentage of G2-M cells, accompanied by an under-tetraploid population, was also observed in the neocortex of E14.5 *Citron-K*$^{-/-}$ embryos (Figure 6A). To further assess if the increase of tetraploid cells in *Citron-K*$^{-/-}$ brains might be caused by a block of cytokinesis, single-cell suspensions from P12 +/+ and −/− cerebellum were plated on polylysine-coated coverslips and analyzed by double immunofluorescence with propidium iodide and anti-β-tubulin antibodies. We found that the

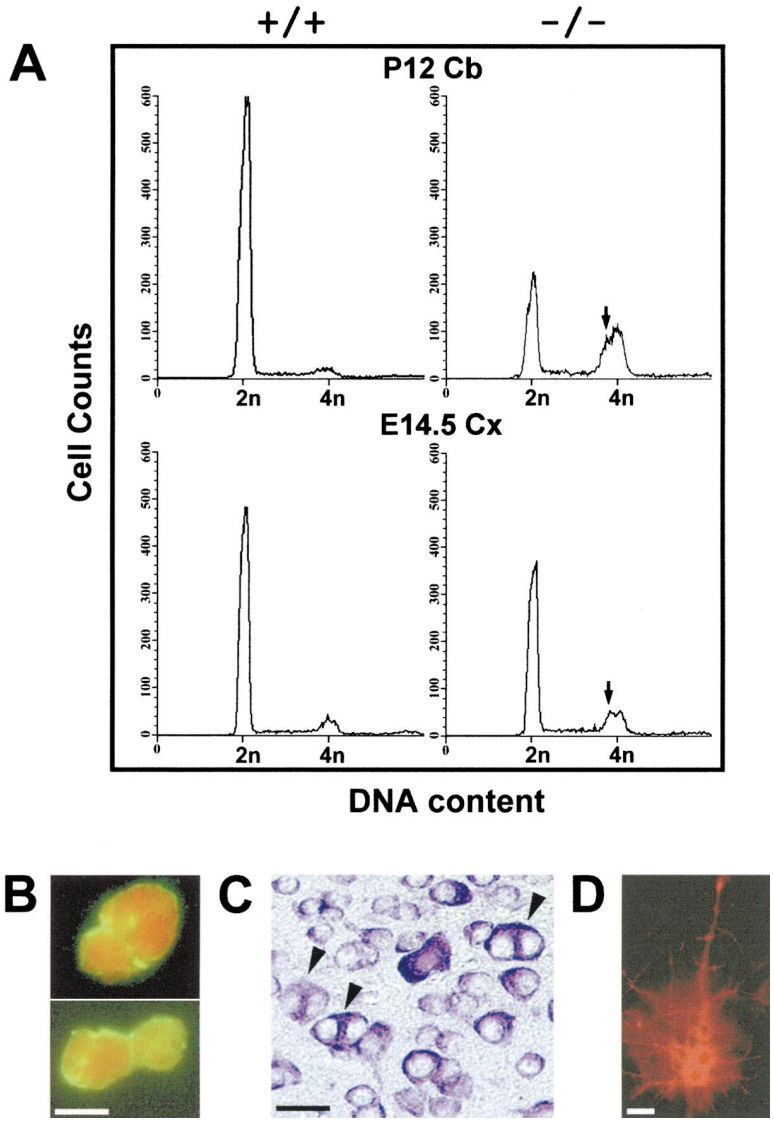


Figure 6. Defective Cytokinesis in Brains of *Citron-K*$^{-/-}$ Mice

(A) Flow cytometric analysis of DNA content performed on single-cell suspensions of P12 cerebellum (Cb) and E14.5 neocortex (Cx) of *Citron-K* +/+ and −/− mice. Arrows indicate the under-tetraploid cell population recognizable in *Citron-K*$^{-/-}$ samples.

(B) Single cells in cytokinesis from P12 *Citron-K*$^{-/-}$ cerebellum.

(C) High power field of P12 *Citron-K*$^{-/-}$ cerebral cortex. Arrowheads point to binucleated cells.

(D) Single binucleated cortico-thalamic pyramidal neuron retrogradely labeled by DiI. Scale bars: 25 μm (C); 10 μm (C); 5 μm (B).

average size of *Citron-K*$^{-/-}$ nuclei was consistently increased and that 5% of them had frankly atypical, plurilobated shapes (data not shown). Moreover, ~10% of the cells displayed a binucleated morphology typical of cytokinesis that could be detected in only 1% of control cells (Figure 6B).

Interestingly, flow cytometric analysis of postnatal cerebral cortex revealed that the amount of tetraploid cells in *Citron-K*$^{-/-}$ samples was significantly increased over controls (4.2% versus 2.3%, respectively, $p < 0.005$). Accordingly, many binucleated cells were identified in sections of P12 −/− cerebral cortex, especially in the deep cortical layers (Figure 6C). Most of them displayed a neuronal morphology on cresyl violet-stained sections and were positively labeled by neurofilament immunohistochemistry (data not shown). The presence of binucleated pyramidal neurons, displaying normal morphology and connectivity, was further confirmed by DiI retrograde labeling of cortico-thalamic projections (Figure 6D). Moreover, BrdU birth-dating experiments indicated that binucleated cells are generated at embryonic stages consistent with their final cortical position (data not shown).

### Apoptotic Cell Death of *Citron-K*$^{-/-}$ Neuronal Precursors Occurs in Tetraploid Cells and Is Associated with Elevated Levels of Cyclin D1

To better establish if the cytokinesis defect and the massive apoptosis identified in the developing brains of *Citron-K*$^{-/-}$ mice are related phenomena, single-cell suspensions from +/+ and −/− cerebellum were analyzed for Caspase-3 activation and DNA content by flow cytometry.

As expected, a strong increase in the total number of Caspase-3-positive cells was detected with this system in the −/− samples (Figure 7A). Strikingly, simultaneous measurement of the DNA content revealed that most of the positive cells were tetraploid, thus indicating that

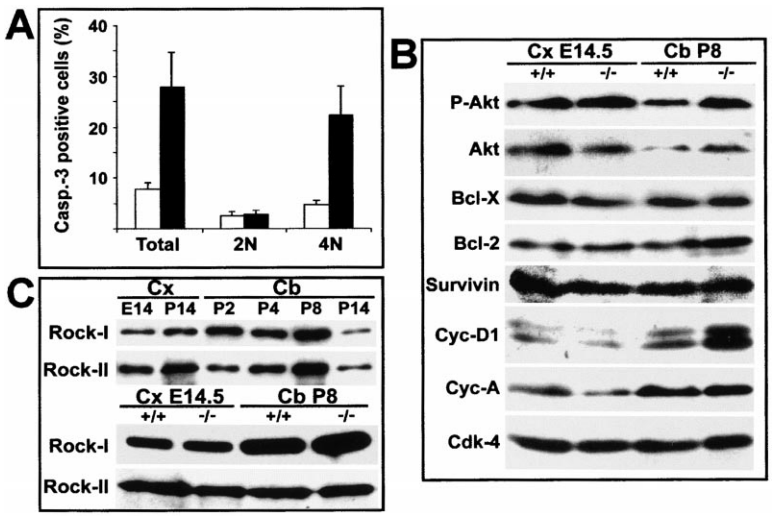


Figure 7. Mechanisms of Apoptotic Cell Death and Expression of ROCKs in *Citron-K*$^{-/-}$ Brains

(A) Flow cytometric measurement of DNA content and activated Caspase-3 positivity in single-cell suspensions from P12 cerebella of *Citron-K* +/+ (open bars) and −/− (closed bars) mice. Error bars = standard deviation.

(B) Western blotting, performed with the indicated antibodies on total cell lysates of *Citron-K* +/+ and −/− developing neocortex and cerebellum.

(C) Measurement of ROCK-I and ROCK-II protein levels on wild-type cortex and cerebellum at the indicated stages (upper panel). Comparison of ROCK-I and ROCK-II protein levels in the developing neocortex and cerebellum of *Citron-K* +/+ and −/− mice (lower panel). The total amount of proteins loaded on each lane was 30 μg.

the apoptotic process is initiated in cells displaying the abnormal cytokinesis phenotype (Figure 7A).

In order to investigate the molecular mechanisms underlying the induction of apoptosis in *Citron-K*$^{-/-}$ neuroblasts, the level of different proteins previously implicated in this process was measured in the developing neocortex and cerebellum of +/+ and −/− mice.

The expression of proteins promoting cell survival, such as Akt and its Thr-308-phosphorylated isoform (Downward, 1998), Bcl-X (Motoyama et al., 1995), Bcl-2 (Michaelidis et al., 1996), and Survivin (Li et al., 1999), was not decreased in −/− samples (Figure 7B). If anything, a slight increase of Akt and Bcl-2 was detected in −/− cerebellum. No significant differences were observed for Cyclin-A, Cdk-4 (Figure 7B), p53, Bax, p21(WAF1/CIP1), and p27 (data not shown). By contrast, a striking increase of Cyclin-D1 was detected in developing −/− cerebellum. Accordingly, immunohistochemical analysis showed that in −/− mice Cyclin D1 was expressed by most of the cerebellar EGL cells (data not shown).

Interestingly, a similar induction of Cyclin-D1 was not detectable in the developing telencephalon (Figure 7B).

### Rho-Kinases Are Expressed at High Levels in Proliferating Neuronal Precursors

Previous studies suggested that ROCKs may regulate cytokinesis downstream of Rho at the level of Citron-K (Goto et al., 1998; Kosako et al., 1997, 1999; Kawano et al., 1999). For this reason, with the aim of better understanding the tissue specificity of Citron-K requirement, we asked if the cell types undergoing cytokinesis block in *Citron-K*$^{-/-}$ are devoid of ROCKs expression.

ROCK-I and ROCK-II protein levels were measured in the neocortex and cerebellum of Citron-K +/+ and −/− mice at different developmental stages. Robust expression of both molecules was detected throughout brain development (Figure 7C). In the cerebellum, the highest levels were detected during the time window of granular cell proliferation (Figure 7C). Accordingly, immunohistochemical analysis revealed strong positivity of the EGL cells (data not shown). At every analyzed stage, no differences were observed between *Citron-K* +/+ and −/− samples for ROCKs expression (Figure 7C) or intracellular localization (data not shown).

## Discussion

In the present report, we analyzed the consequences of Citron-K deficiency on mouse development.

A potential complication for this study was the production of two different isoforms by the *Citron-K* transcription unit. However, the gene-targeting strategy that we devised resulted in the complete loss of Citron-K and had no effects on Citron-N expression (Figure 2E).

The biologic functions of Citron-N remain to be elucidated. It is composed of the same domains of Citron-K with the exception of the kinase domain. Therefore, it could compete for binding to activated Rho and act as an endogenous inhibitor of Citron-K function. However, this mechanism is unlikely to play a role in producing the phenotype of *Citron-K*$^{-/-}$ mice, since the observed cellular defects arise at developmental stages characterized by negligible expression of Citron-N (Figure 1C).

### Citron-K Is a Tissue-Specific and Nonredundant Regulator of Cytokinesis

Rho is known to be essential for the acto-myosin ring that drives cytokinesis in eukaryotic cells (Kishi et al., 1993; Drechsel et al., 1997; Nakano et al., 1997), but the molecular events that follow its activation are still controversial. Several studies have suggested a role for the ROCKs as downstream effectors of Rho in this process (Kosako et al., 1997, 1999; Goto et al., 1998; Kawano et al., 1999). Indeed, during cytokinesis, these molecules colocalize with the cleavage furrow and the midbody (Kosako et al., 1999), where they appear to phosphorylate MBS (Kawano et al., 1999) and intermediate filaments (Kosako et al., 1997; Goto et al., 1998). However, a different report (Madaule et al., 1998), based on in vitro overexpression of mutants and pharmacological inhibition, suggested that Rho-kinases play a minor functional role in cytokinesis and proposed Citron-K as the crucial downstream effector.

In this study we have demonstrated that Citron-K is required for cytokinesis in vivo. However, our data indicate that this requirement is restricted to specialized cell types. Indeed Citron-K expression is remarkably tissue- and developmental stage-specific (Di Cunto et al., 1998) (Figure 1). Moreover, loss of Citron-K had no effects on cytokinesis in many tissues that express it at significant levels. Between the analyzed cell types, only a subset of neuronal precursors required Citron-K to complete cytokinesis (Figure 6). Taken together, these evidences indicate that other molecules must be implicated in regulating cytokinesis downstream of Rho at the level of Citron-K.

Based on the above-mentioned reports and given their structural similarity with Citron-K, ROCKs would be the most obvious candidates. According to this assumption, loss of Citron-K would be predicted to functionally affect cytokinesis only in cells devoid of ROCKs. However, we found strong expression of ROCK-I and ROCK-II in *Citron-K* +/+ and −/− proliferating telencephalon and cerebellum (Figure 7C). In particular, significant expression of both molecules was detected by immunohistochemistry in cerebellar granule precursors of the EGL (data not shown), which are one of the cell types most severely compromised in *Citron-K*$^{-/-}$ mice.

These data strongly indicate that, at least in specific neuronal precursors, Citron-K regulates cell type–specific aspects of cytokinesis, which cannot be covered by related molecules. It is noteworthy that cells displaying the highest sensitivity to the absence of Citron-K are the precursors of the olfactory bulb, hippocampal and cerebellar granules, which are generated from secondary germinal matrices and share common functional, morphologic, and molecular features (Hatten et al., 1997). The extreme tissue specificity of Citron-K requirement will be probably better understood after identification of its downstream targets.

### Mechanisms of Apoptotic Cell Death Induction in *Citron-K*$^{-/-}$ Neuroblasts

Although in *Citron-K*$^{-/-}$ neocortex a significant number of tetraploid neurons is able to survive and complete the differentiation program, the observed cytokinesis defect was usually associated with induction of apoptosis. This would suggest that failure to complete cytokinesis might activate homeostatic responses similar to the G2-M and spindle checkpoints (Li et al., 1998, 1999; Mercer, 1998), resulting most of the time in programmed cell death.

Alternatively, Citron-K could be independently required in the affected cell types for cytokinesis and for a specific cell survival pathway.

According to the first hypothesis, we detected in developing cerebellum and telencephalon of *Citron-K*$^{-/-}$ mice an under-tetraploid population, likely corresponding to cells blocked in cytokinesis and undergoing apoptotic DNA degradation. More significantly, we found that most of the cells displaying Caspase-3 activation have a tetraploid DNA content, thus indicating that the apoptotic process is initiated in the cytokinesis-deficient cells. Moreover, the expression levels of proteins associated with specific cell survival pathways were not decreased in developing *Citron-K*$^{-/-}$ brains. Although the existence of an unknown cell survival pathway requiring Citron-K cannot be yet excluded, the available evidences strongly suggest that the apoptotic cell death of *Citron-K*$^{-/-}$ neuroblast is a direct consequence of the cytokinesis block.

The molecular mechanisms responsible for sensing the cell division defect and activating the caspase cascade remain to be characterized.

However, we have found that *Citron-K*$^{-/-}$ cerebellar EGL precursors express very high levels of Cyclin-D1 (Figure 7B and data not shown), which has been previously reported as an essential mediator of apoptotic cell death in postmitotic neurons (Kranenburg et al., 1996). This result could not be simply explained by a relative increase of the proliferating cell fraction due to depletion of the postmitotic compartment. Indeed, levels of the proliferation markers Cyclin-A and Cdk-4 were not significantly different in +/+ and −/− samples.

Overexpression of Cyclin-D1 by cells blocked in the M phase of the cell cycle could be among the effector mechanisms of the cell death program. Alternatively, it could indicate a severe deregulation of the cell cycle that may ultimately lead to apoptotic cell death. In both cases, induction of apoptosis could be the result of an aborted attempt to start the cell division cycle in tetraploid cells, as previously proposed for postmitotic neurons (Kranenburg et al., 1996).

Interestingly, increased levels of Cyclin D1 were not detectable in the developing neocortex. This could be justified by the much lower fraction of cortical cells displaying impaired cytokinesis and apoptosis (Figure 6A). Alternatively, it might reflect intrinsic differences between cerebellar and neocortical precursors, which could partially protect the latter from apoptosis and allow them to completely differentiate as binucleated neurons.

### *Citron-K*-Deficient Mice Display a Specific Neurological Syndrome, Similar to a Subset of Recessive Lissencephalies

*Citron-K*$^{-/-}$ mice die before reaching adulthood, most likely due to lethal epilepsy. Accordingly, they displayed reduced threshold and abnormal sensitivity to seizures induced by the chemical convulsant PTZ. Although failure to thrive was also apparent, there was no correlation between mortality and growth rate.

The cerebral defects observed in *Citron-K*$^{-/-}$ mice represent a fairly good explanation for their neurological symptoms. In particular, as in many other mutant mice (Patil et al., 1995; Miyata et al., 1999; Rice and Curran, 1999), the ataxia could be explained by the severe cerebellar abnormalities. On the other hand, the abnormal cortical structure, the strong reduction of GABA-ergic interneurons and the absence of the hippocampal dentate gyrus may all contribute to the genesis of lethal seizures (Puranam and McNamara, 1999).

The neurological syndrome of *Citron-K*$^{-/-}$ mice displays striking similarities to human autosomic recessive lissencephalies with hypotrophic cerebellum (Walsh, 1999; Whiting and Duchowny, 1999), whose genetic basis are almost completely unknown. Our study indicates that inactivation of genes involved in the control of cytokinesis could be one of the possible molecular causes

for at least some of these severe malformative syndromes. Moreover, *Citron-K*$^{-/-}$ mice provide a useful experimental model for such pathologic conditions.

## Experimental Procedures

### In Situ Hybridization

ISH was performed as described (Broccoli et al., 1999), with antisense RNA probes transcribed from plasmids containing fragments of *Citron-K* (Di Cunto et al., 1998) (nucleotides 911–2056 for probe K and 2560–3581 for probe C), *Id-2* (Bulfone et al., 1995), *Dlx-2* (Anderson et al., 1997), and *NeuroD* (EST clone ID, W97999).

### Generation of *Citron-K* Mutant Mice

A mouse genomic clone, containing the 5′ region of *Citron-K*, was isolated from a 129Sv BAC library. Two restriction fragments containing the 5′ and the 3′ halves of the second coding exon, along with 4.2 kb and 5.4 kb of flanking DNA, respectively, were subcloned in pWH9 (kindly provided by Dr. R. Fässler). In this way, a β-Gal-PGK-Neo cassette was inserted in a sense orientation, in the second coding exon, 144 bp downstream of the initiator ATG. The targeting vector was linearized at a unique NotI site. R1 ES cells were transfected with the targeting construct and selected in G418-containing media. Southern blotting with probe A of genomic DNA from 230 resistant clones showed that two of them had undergone homologous recombination. Positive clones were also analyzed with probe B and with a Neo-specific probe to confirm correct integration of the construct. Both clones were injected into C57Bl/6 blastocysts, and male chimeras displaying 100% agouti coat were mated to C57BL/6 and 129Sv females to produce outbred and inbred F1 heterozygous offspring. The described phenotypes were observed in mice derived from both ES cell clones. All the experiments shown were performed on 129/Sv inbred lines. No phenotypic differences were observed between inbred and 129Sv × C57Bl/6 lines at the third generation of outbreeding. Routine determination of genotypes was performed by PCR with oligonucleotides derived from sequences flanking the targeted exon and from the Neo poly(A) (Figure 2B).

### Western Blotting

Tissues were homogenized in 2× SDS sample buffer (65 mM Tris-HCl [pH 6.8], 2% SDS, 10% glycerol) and incubated for 4 min at 95&z.ousco;C. Western blotting was performed essentially as described (Di Cunto et al., 1998). The anti-Citron-K polyclonal antiserum was raised by immunization of rabbits with amino acids 454–637 and used at 1:2000 dilution. Monoclonal antibodies against ROCK-I and ROCK-II were purchased by Transduction Laboratories and used according to the manufacturer's specifications. Polyclonal antibodies against Bcl-X, Bcl-2, Survivin, Cyclin-D1, Cyclin A, Cdk-4, p53, Bax, p21(WAF1/CIP1), and p27 were purchased from Santa Cruz and used at 1:1000 dilution. Antibodies against Akt and Thr-308-phospho-Akt were purchased from NEB and used according to the manufacturer's specifications. The results shown are representative of at least three independent experiments.

### PTZ Seizure Induction

P12 control and *Citron-K*$^{-/-}$ mice were injected intraperitoneally with PTZ (Sigma) at 40 mg/kg body weight. Observations were made during the 2 hr period immediately following injection. All surviving mice were euthanized the day after PTZ injection. Data reported in the text were obtained in two independent experiments.

### Histology and Quantitative Analysis

Embryos were fixed by immersion in fixative solution (4% paraformaldehyde in PBS). Postnatal mice were deeply anaesthetized and transcardially perfused with fixative solution. Brains and other organs were removed, postfixed for at least 12 hr, embedded in paraffin, and sectioned at 5 μm. Brain sections were stained with hematoxilin-eosin (H&E) and cresyl violet. Sections of other organs were stained with H&E. DiI labeling was performed as described (Vercelli et al., 2000).

Quantitative measurement of cortical cell numbers was performed on 20× magnification photomicrographs of comparable coronal sections from each genotype using the free UTHSCSA ImageTool program (developed at the University of Texas Health Science Center at San Antonio, Texas and available from the Internet by anonymous FTP from ftp://maxrad6.uthscsa.edu). The number of mice in each experiment was five per genotype. Statistical significance of differences between *Citron-K*$^{-/-}$ and control samples was assessed by the Student's t test.

### Immunohistochemistry

TUNEL assay was performed as previously described (Migheli et al., 1999). Activated Caspase-3 was detected with an affinity-purified rabbit polyclonal antiserum, which recognizes the p17 subunit of cleaved Caspase-3 (kindly provided by Dr. A. Nelsbach, NEB, Beverly, MA). For BrdU immunostaining, mice were labeled with a single injection of BrdU (Sigma) at 100 mg/kg and sacrificed after 1 hr (for determination of the proliferative index) or at P8 (for neuronal birth-dating experiments). Tissues were fixed in Carnoi, embedded in paraffin, and sectioned at 5 μm. After rehydration sections were treated for 20 min with 1 M HCl. Anti-BrdU antibodies (Chemicon) were used at 1:100 dilution. The other immunostainings were performed as described (Migheli et al., 1999) using the following antibodies: anti-calretinin monoclonal (Chemicon), 1:1000; anti-calbindin polyclonal (Chemicon), 1:2000; anti-activated Caspase-3, 1:1000; anti-ROCK-I and -ROCK-II (Transduction Laboratories), 1:100; anti-neurofilaments (Chemicon), 1:1000; and anti-Cyclin D1, 1:1000 (Santa Cruz). The number of mice in each experiment was three per genotype.

### Flow Cytometric Analysis

Tissues from embryos or postnatal mice were dissociated by mechanical trituration in PBS, and single-cell suspensions obtained by filtering through 70 μm nylon mesh. Determination of the DNA content ($n = 5$ for each genotype and developmental stage) was performed using the Cycle Test Plus kit (Becton Dickinson) according to the manufacturer's specifications. For the simultaneous determination of DNA content and activated Caspase-3 levels ($n = 3$ for each genotype) cells were fixed overnight in 70% ethanol. After washing twice in PBS, $10^6$ cells were permeabilized with 200 μl of solution B from the above-mentioned kit and sequentially incubated for 45 min with anti-activated Caspase-3, fluoresceinated secondary antibodies, and solution C. After the last incubation samples were filtered through 30 μm nylon mesh and 20,000 events were collected on a FACScalibur station (Becton Dickinson). Quantitative analysis of cell cycle parameters was performed using Mod-Fit program. Statistical significance of differences between *Citron-K*$^{-/-}$ and control samples was assessed by the Student's t test.

### Analysis of Dissociated Cerebellar Cells

Cerebella from P8 mice ($n = 3$) were mechanically dissociated in DMEM, and single-cell suspension were obtained by sequential filtering through 70 μm and 30 μm nylon mesh. Cells were left to adhere for 15 min onto polylysine-coated coverslips and fixed for 5 min with 2% paraformaldehyde in PBS. Samples were then analyzed by immunofluorescence after labeling with anti-β-tubulin FITC antibodies (Sigma; 1:50 in PBS) and propidium iodide (Sigma; 2 μg/ml).

### Acknowledgments

We thank M. Ghiani and C. Gattuso for technical support with the ISH experiments; A. Nagy for providing R1 ES cells; J. L. R. Rubenstein and M. A. Israel for the *Dlx-2* and *Id-2* probes, respectively; A. Vercelli for the DiI labeling experiments; and P. Camera, G. Topley, M. Enrietto, and L. Ferrara for excellent technical assistance. This work was supported by grant 405/bi from Comitato Telethon Fondazione Onlus to F. D. C.; by National Institutes of Health Grants AR39190, CA16038, and CA73796 and, in part, by the CBRC through the MGH/Shiseido Co. Ltd. Agreement to G. P. D.; by Contributo CNR Programma Biotecnologie to L. S.; and by P. F. Biotecnologie CNR and MURST Cofin99 to F. A.

Received May 12, 2000; revised August 18, 2000.

## References

Anderson, S.A., Eisenstat, D.D., Shi, L., and Rubenstein, J.L. (1997). Interneuron migration from basal forebrain to neocortex: dependence on Dlx genes. Science *278*, 474–476.

Barrett, K., Leptin, M., and Settleman, J. (1997). The Rho GTPase and a putative RhoGEF mediate a signaling pathway for the cell shape changes in Drosophila gastrulation. Cell *91*, 905–915.

Broccoli, V., Boncinelli, E., and Wurst, W. (1999). The caudal limit of Otx2 expression positions the isthmic organizer. Nature *401*, 164–168.

Bulfone, A., Smiga, S.M., Shimamura, K., Peterson, A., Puelles, L., and Rubenstein, J.L. (1995). T-brain-1: a homolog of Brachyury whose expression defines molecularly distinct domains within the cerebral cortex. Neuron *15*, 63–78.

Bulfone, A., Wang, F., Hevner, R., Anderson, S., Cutforth, T., Chen, S., Meneses, J., Pedersen, R., Axel, R., and Rubenstein, J.L. (1998). An olfactory sensory map develops in the absence of normal projection neurons or GABAergic interneurons. Neuron *21*, 1273–1282.

Chae, T., Kwon, Y.T., Bronson, R., Dikkes, P., Li, E., and Tsai, L.H. (1997). Mice lacking p35, a neuronal specific activator of Cdk5, display cortical lamination defects, seizures, and adult lethality. Neuron *18*, 29–42.

Di Cunto, F., Calautti, E., Hsiao, J., Ong, L., Topley, G., Turco, E., and Dotto, G.P. (1998). Citron rho-interacting kinase, a novel tissue-specific ser/thr kinase encompassing the Rho-Rac-binding protein Citron. J. Biol. Chem. *273*, 29706–29711.

Downward, J. (1998). Mechanisms and consequences of activation of protein kinase B/Akt. Curr. Opin. Cell Biol. *10*, 262–267.

Drechsel, D.N., Hyman, A.A., Hall, A., and Glotzer, M. (1997). A requirement for Rho and Cdc42 during cytokinesis in Xenopus embryos. Curr. Biol. *7*, 12–23.

Furuyashiki, T., Fujisawa, K., Fujita, A., Madaule, P., Uchino, S., Mishina, M., Bito, H., and Narumiya, S. (1999). Citron, a Rho-target, interacts with PSD-95/SAP-90 at glutamatergic synapses in the thalamus. J. Neurosci. *19*, 109–118.

Goldowitz, D., and Hamre, K. (1998). The cells and molecules that make a cerebellum. Trends Neurosci. *21*, 375–382.

Goto, H., Kosako, H., Tanabe, K., Yanagida, M., Sakurai, M., Amano, M., Kaibuchi, K., and Inagaki, M. (1998). Phosphorylation of vimentin by Rho-associated kinase at a unique amino-terminal site that is specifically phosphorylated during cytokinesis. J. Biol. Chem. *273*, 11728–11736.

Hall, A. (1998). Rho GTPases and the actin cytoskeleton. Science *279*, 509–514.

Hatten, M.E., Alder, J., Zimmerman, K., and Heintz, N. (1997). Genes involved in cerebellar cell specification and differentiation. Curr. Opin. Neurobiol. *7*, 40–47.

Hinds, J.W. (1968). Autoradiographic study of histogenesis in the mouse olfactory bulb. II. Cell proliferation and migration. J. Comp. Neurol. *134*, 305–322.

Kawano, Y., Fukata, Y., Oshiro, N., Amano, M., Nakamura, T., Ito, M., Matsumura, F., Inagaki, M., and Kaibuchi, K. (1999). Phosphorylation of myosin-binding subunit (MBS) of myosin phosphatase by Rho-kinase in vivo. J. Cell Biol. *147*, 1023–1038.

Kishi, K., Sasaki, T., Kuroda, S., Itoh, T., and Takai, Y. (1993). Regulation of cytoplasmic division of Xenopus embryo by rho p21 and its inhibitory GDP/GTP exchange protein (rho GDI). J. Cell Biol. *120*, 1187–1195.

Kosako, H., Amano, M., Yanagida, M., Tanabe, K., Nishi, Y., Kaibuchi, K., and Inagaki, M. (1997). Phosphorylation of glial fibrillary acidic protein at the same sites by cleavage furrow kinase and Rho-associated kinase. J. Biol. Chem. *272*, 10333–10336.

Kosako, H., Goto, H., Yanagida, M., Matsuzawa, K., Fujita, M., Tomono, Y., Okigaki, T., Odai, H., Kaibuchi, K., and Inagaki, M. (1999). Specific accumulation of Rho-associated kinase at the cleavage furrow during cytokinesis: cleavage furrow-specific phosphorylation of intermediate filaments. Oncogene *18*, 2783–2788.

Kranenburg, O., van der Eb, A.J., and Zantema, A. (1996). Cyclin D1 is an essential mediator of apoptotic neuronal cell death. EMBO J. *15*, 46–54.

Lee, T., Winter, C., Marticke, S.S., Lee, A., and Luo, L. (2000). Essential roles of Drosophila RhoA in the regulation of neuroblast proliferation and dendritic but not axonal morphogenesis. Neuron *25*, 307–316.

Leung, T., Chen, X.Q., Manser, E., and Lim, L. (1996). The p160 RhoA-binding kinase ROK alpha is a member of a kinase family and is involved in the reorganization of the cytoskeleton. Mol. Cell. Biol. *16*, 5313–5327.

Li, F., Ambrosini, G., Chu, E.Y., Plescia, J., Tognin, S., Marchisio, P.C., and Altieri, D.C. (1998). Control of apoptosis and mitotic spindle checkpoint by survivin. Nature *396*, 580–584.

Li, F., Ackermann, E.J., Bennett, C.F., Rothermel, A.L., Plescia, J., Tognin, S., Villa, A., Marchisio, P.C., and Altieri, D.C. (1999). Pleiotropic cell-division defects and apoptosis induced by interference with survivin function. Nat. Cell Biol. *1*, 461–466.

Luo, L., Liao, Y.J., Jan, L.Y., and Jan, Y.N. (1994). Distinct morphogenetic functions of similar small GTPases: Drosophila Drac1 is involved in axonal outgrowth and myoblast fusion. Genes Dev. *8*, 1787–1802.

Luo, L., Hensch, T.K., Ackerman, L., Barbel, S., Jan, L.Y., and Jan, Y.N. (1996). Differential effects of the Rac GTPase on Purkinje cell axons and dendritic trunks and spines. Nature *379*, 837–840.

Luo, L., Jan, L.Y., and Jan, Y.N. (1997). Rho family GTP-binding proteins in growth cone signaling. Curr. Opin. Neurobiol. *7*, 81–86.

Madaule, P., Furuyashiki, T., Reid, T., Ishizaki, T., Watanabe, G., Morii, N., and Narumiya, S. (1995). A novel partner for the GTP-bound forms of rho and rac. FEBS Lett. *377*, 243–248.

Madaule, P., Eda, M., Watanabe, N., Fujisawa, K., Matsuoka, T., Bito, H., Ishizaki, T., and Narumiya, S. (1998). Role of citron kinase as a target of the small GTPase Rho in cytokinesis. Nature *394*, 491–494.

Magie, C.R., Meyer, M.R., Gorsuch, M.S., and Parkhurst, S.M. (1999). Mutations in the Rho1 small GTPase disrupt morphogenesis and segmentation during early Drosophila development. Development *126*, 5353–5364.

Matsui, T., Amano, M., Yamamoto, T., Chihara, K., Nakafuku, M., Ito, M., Nakano, T., Okawa, K., Iwamatsu, A., and Kaibuchi, K. (1996). Rho-associated kinase, a novel serine/threonine kinase, as a putative target for small GTP binding protein Rho. EMBO J. *15*, 2208–2216.

Mercer, W.E. (1998). Checking on the cell cycle. J. Cell. Biochem. *30–31* (*suppl.*), 50–54.

Michaelidis, T.M., Sendtner, M., Cooper, J.D., Airaksinen, M.S., Holtmann, B., Meyer, M., and Thoenen, H. (1996). Inactivation of bcl-2 results in progressive degeneration of motoneurons, sympathetic and sensory neurons during early postnatal development. Neuron *17*, 75–89.

Migheli, A., Piva, R., Casolino, S., Atzori, C., Dlouhy, S.R., and Ghetti, B. (1999). A cell cycle alteration precedes apoptosis of granule cell precursors in the weaver mouse cerebellum. Am. J. Pathol. *155*, 365–373.

Miyata, T., Maeda, T., and Lee, J.E. (1999). NeuroD is required for differentiation of the granule cells in the cerebellum and hippocampus. Genes Dev. *13*, 1647–1652.

Motoyama, N., Wang, F., Roth, K.A., Sawa, H., Nakayama, K., Negishi, I., Senju, S., Zhang, Q., Fujii, S., et al. (1995). Massive cell death of immature hematopoietic cells and neurons in Bcl-x-deficient mice. Science *267*, 1506–1510.

Nakagawa, O., Fujisawa, K., Ishizaki, T., Saito, Y., Nakao, K., and Narumiya, S. (1996). ROCK-I and ROCK-II, two isoforms of Rho-associated coiled-coil forming protein serine/threonine kinase in mice. FEBS Lett. *392*, 189–193.

Nakano, K., Arai, R., and Mabuchi, I. (1997). The small GTP-binding protein Rho1 is a multifunctional protein that regulates actin localization, cell polarity, and septum formation in the fission yeast Schizosaccharomyces pombe. Genes Cells *2*, 679–694.

Narumiya, S. (1996). The small GTPase Rho: cellular functions and signal transduction. J. Biochem. *120*, 215–228.

Narumiya, S., Ishizaki, T., and Watanabe, N. (1997). Rho effectors and reorganization of actin cytoskeleton. FEBS Lett. *410*, 68–72.

Patil, N., Cox, D.R., Bhat, D., Faham, M., Myers, R.M., and Peterson, A.S. (1995). A potassium channel mutation in weaver mice implicates membrane excitability in granule cell differentiation. Nat. Genet. *11*, 126–129.

Puranam, R.S., and McNamara, J.O. (1999). Seizure disorders in mutant mice: relevance to human epilepsies. Curr. Opin. Neurobiol. *9*, 281–287.

Rice, D.S., and Curran, T. (1999). Mutant mice with scrambled brains: understanding the signaling pathways that control cell positioning in the CNS. Genes Dev. *13*, 2758–2773.

Srinivasan, A., Roth, K.A., Sayers, R.O., Shindler, K.S., Wong, A.M., Fritz, L.C., and Tomaselli, K.J. (1998). In situ immunodetection of activated caspase-3 in apoptotic neurons in the developing nervous system. Cell Death Differ. *5*, 1004–1016.

Steven, R., Kubiseski, T.J., Zheng, H., Kulkarni, S., Mancillas, J., Morales, A.R., Hogue, C.W.V., Pawson, T., and Culotti, J. (1998). UNC-73 activates the rac GTPase and is required for cell and growth cone migrations in *C. Elegans*. Cell *92*, 785–795.

Sugihara, K., Nakatsuji, N., Nakamura, K., Nakao, K., Hashimoto, R., Otani, H., Sakagami, H., Kondo, H., Nozawa, S., Aiba, A., and Katsuki, M. (1998). Rac1 is required for the formation of three germ layers during gastrulation. Oncogene *17*, 3427–3433.

Valencia, A., Chardin, P., Wittinghofer, A., and Sander, C. (1991). The ras protein family: evolutionary tree and role of conserved amino acids. Biochemistry *30*, 4637–4648.

Van Aelst, L., and D'Souza-Schorey, C. (1997). Rho GTPases and signaling networks. Genes Dev. *11*, 2295–2322.

Vercelli, A., Repici, M., Garbossa, D., and Grimaldi, A. (2000). Recent techniques for tracing pathways in the central nervous system of developing and adult mammals. Brain Res. Bull. *51*, 11–28.

Walsh, C.A. (1999). Genetic malformations of the human cerebral cortex. Neuron *23*, 19–29.

Whiting, S., and Duchowny, M. (1999). Clinical spectrum of cortical dysplasia in childhood: diagnosis and treatment issues. J. Child Neurol. *14*, 759–771.

Wunnenberg-Stapleton, K., Blitz, I.L., Hashimoto, C., and Cho, K.W. (1999). Involvement of the small GTPases XRhoA and XRnd1 in cell adhesion and head formation in early Xenopus development. Development *126*, 5339–5351.

Yasui, Y., Amano, M., Nagata, K., Inagaki, N., Nakamura, H., Saya, H., Kaibuchi, K., and Inagaki, M. (1998). Roles of Rho-associated kinase in cytokinesis; mutations in Rho-associated kinase phosphorylation sites impair cytokinetic segregation of glial filaments. J. Cell Biol. *143*, 1249–1258.

Zhang, W., Vazquez, L., Apperson, M., and Kennedy, M.B. (1999). Citron binds to PSD-95 at glutamatergic synapses on inhibitory neurons in the hippocampus. J. Neurosci. *19*, 96–108.